(23)

(76-235)

STUDY OF ARCTIC SEA ICE DRIFT FROM L-BAND SYNTHETIC APERTURE RADAR*

F. Leberl,** T. Farr, L. Bryan, and C. Elachi

Space Sciences Division
Jet Propulsion Laboratory
California Institute of Technology
Pasadena, California 91103

BIOGRAPHICAL SKETCHES

Franz Leberl graduated as a geodesist from the Technological University of Vienna, Austria, with a doctorate in the applied sciences. Prior to coming to California, he was employed by the International Institute for Aerial Surveys and Earth Sciences (ITC) in the Netherlands.

Tom Farr received a BS in geology from California Institute of Technology and is presently a graduate student of that University.

Len Bryan received his Ph.D in geography from the University of Michigan. He worked at the Environmental Research Institute of Michigan (ERIM) on problems of radar interpretation prior to joining JPL.

Charles Elachi holds a Ph.D in electrical engineering from the California Institute of Technology and is presently the Supervisor of the Radar Science and Applications Group at JPL.

ABSTRACT

As part of the Arctic Ice Dynamics Joint Experiment (AIDJEX) several repetitive coverages of L-band (25 cm wavelength) side-looking airborne radar images have been flown over coastal areas of Alaska and a test area in the Arctic. These images allow the analysis of sea ice and its drift. Radar is particularly suited for the mapping and interpretation of Arctic sea ice due to independence from sunlight and the capability to penetrate clouds. Ice floes and leads can be readily identified on the radar images. Measurement of ice floe drift is based on the transformation of radar image coordinates into a geocentric coordinate system using inertial guidance data from the survey aircraft.

The paper will demonstrate an example of Arctic ice drift measurements from L-band synthetic aperture radar imagery with an absolute accuracy of about 5%. The conclusions are of particular value in view of planned spaceborne side-looking radar missions in polar orbits.

1. INTRODUCTION

It is generally recognized and has been demonstrated at several occasions that radar can image the distribution of sea ice through clouds, precipitation and in the dark (Campbell et al., 1975). Sea ice occurs in the polar regions which often are cloud covered and where the sun remains below the horizon during part of the year. This and the high resolution of presently up to 3 x 3 m^2 (more commonly 10 x 10 to 25 x 25 m^2) would make radar thus a remote sensing device well suited to provide data on sea ice distribution, drift and differential drift as an input to geo-

*This paper presents the results of one phase of research carried out at JPL, California Institute of Technology, under contract NAS7-100, sponsored by the National Aeronautics and Space Administration.
**NRC Resident Research Associate

physical studies of floating sea ice. In spite of this no reports (in the English language) have come to the attention of the authors, that would describe the use of radar for quantitatively mapping sea ice distributions far from land. To date, sea ice studies with radar address, at least in the United States and Canada, either only coastal areas or limit themselves to qualitative image interpretation (Anderson, 1966; Dunbar, 1975).

The Jet Propulsion Laboratory (JPL) participated during the year 1975 in three flight missions of the Arctic Ice Dynamics Joint Experiment (AIDJEX). The imaging synthetic aperture L-Band (25 cm wavelength) radar system of JPL was used aboard a NASA CV-990 aircraft to provide side-looking radar imagery of the North Slope of Alaska and of Arctic sea ice in the AIDJEX test site. This site is located about 400 km north of Alaska (Fig. 1). Images were produced in April, August and October 1975, thus of winter-, summer- and fall-ice. One of the purposes of participation in the NASA-AIDJEX flights was to analyze and demonstrate the applicability of radar imaging to map and study the dynamics of sea ice far from land, and to gain experience in this mapping effort in view of the orbital radar images which will become available in 1978-79 from the SEASAT spacecraft, which will travel around the Earth in a near polar orbit.

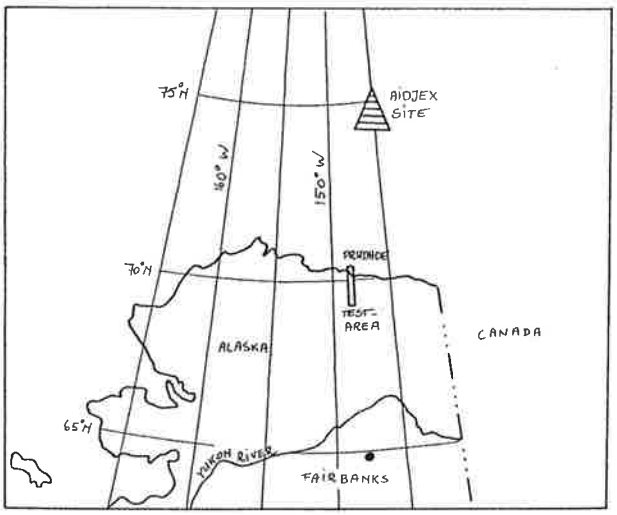

Figure 1:

Geographic location of the AIDJEX test site.

The present paper will present some first results of this analysis of sea ice radar mapping. A method of computing geocentric coordinates from airborne or orbital radar image points is first reviewed. Inputs to the method are measurements of points in the radar images and recordings of the position of the sensor platform. The accuracy of the geocentric coordinates as obtained from the JPL L-Band radar system is analyzed using images of land. Mapping of actual sea ice-distribution and drift is then demonstrated using a pair of individual side-looking airborne radar (SLAR) strips flown at different days over the same part of the AIDJEX test area.

The NASA-AIDJEX flights were devoted to an array of remote sensing experiments, of which radar imaging was but one part. Therefore, the flight plans could not be optimized for radar mapping. As a result, most of the flights did not produce sets of overlapping radar images that could be compiled into mosaics. Rather individual independent image strips were obtained. The navigational discipline and geometric rigidity applied in the image acquisition was not as high as is desirable and possible for sucessful radar mapping. The obtained results are therefore less accurate than one can expect in the best case. However, the absolute accuracy of mapping sea-ice from the radar imagery which was produced during the NASA-AIDJEX flights is similar to the accuracy obtainable from LANDSAT imagery. But the radar resolution is much higher. This would thus suggest that as a tool for mapping micro- and mesoscale sea-ice distribution radar is superior to LANDSAT even in the case of good lighting conditions and the absence of clouds.

2. TRANSFORMATION OF RADAR IMAGE MEASUREMENTS INTO GEOCENTRIC COORDINATES

2.1 Transformation Algorithm

Sea ice drift is defined as the change of position of individual ice features over time. Although ice drift studies usually consider strain, strain rate and vorticity of the ice-sheet, these are in fact only derived from ice drift measurements. In the present context, it is therefore sufficient to only consider sea ice drift. This is measured by comparing sequential maps of the distribution of homologuous sea ice features. A first requirement for the mapping of sea ice drift is thus the transformation of radar image coordinates into a geocentric or geographical system and then into a plane projection of the terrestrial sphere.

An algorithm was originally developed for mapping of the lunar surface from orbital radar images (Leberl, 1975b). This algorithm is also applicable to mapping of arctic sea ice from airborne radar. It is this algorithm with only slight modifications that is used in the present study. Figure 2 shows an example of an L-Band radar image as produced by the JPL system.

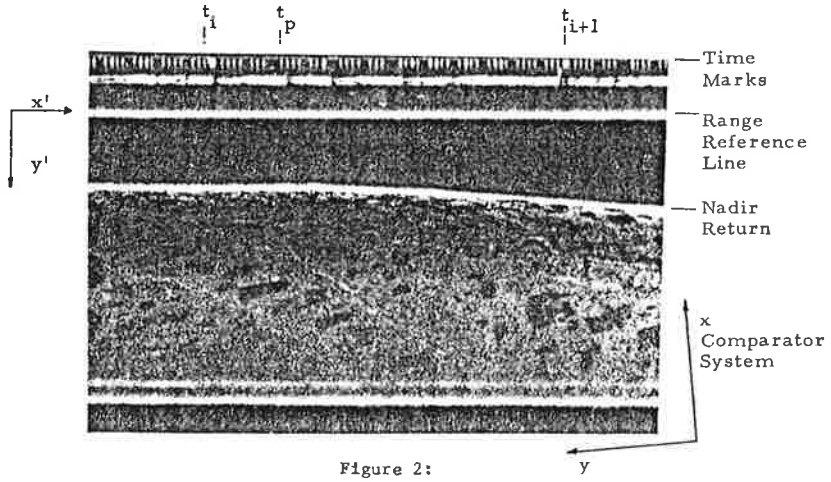

Figure 2:
Example of a side-looking radar image in slant range presentation, produced by the synthetic aperture L-Band system of the Jet Propulsion Laboratory over Prudhoe Bay, Alaska.

The time code and range reference line are being used to transform digital x, y comparator measurements of identifiable ice features into time t_p of imaging this feature and into its range r_p. First the x, y comparator coordinate system is rotated into an x', y' system so that the x'-axis coincides with the time-, and the y'-axis with the range direction. Time t_p and range r_p result then from x', y':

$$t_p = t_i + (x'_{t_p} - x'_{t_i}) \cdot (t_{i+1} - t_i)/(x'_{t_{i+1}} - x'_{t_i}) \qquad (1)$$

$$r_p = (y'_p + c) \cdot f \qquad (2)$$

The sweep delay c and scale factor f have to be available as an input to the radar coordinate transformation. Using time t_p, the aircraft position vector $\underline{s}$ and velocity vector $\dot{\underline{s}}$ can be interpolated from recordings produced from the inertial navigation. Vectors $\underline{s}$, $\dot{\underline{s}}$, slant range r_p and the radius R of the terrestrial sphere are input to an algorithm to compute the geocentric coordinates of the surface point P. One obtains thus from figure 3 (Leberl, 1975b):

$$a = (R^2 + |\underline{s}|^2 - r_p^2)/2 \cdot |\underline{s}| \qquad \cos\phi = \underline{u} \cdot \dot{\underline{s}} / |\dot{\underline{s}}|$$

$$\underline{a} = \underline{s} \cdot a/|\underline{s}| \qquad \underline{b} = \underline{u} \cdot (|\underline{s}| - |\underline{a}|) \cdot \tan\phi$$

$$\underline{w} = (\dot{\underline{s}} \times \underline{s})/(|\dot{\underline{s}} \times \underline{s}|) \qquad g = (|\underline{s}| - |\underline{a}|)^2$$

$$\underline{u} = \underline{w} \times \underline{s} / |\underline{s} \times \underline{w}| \qquad \underline{c} = \underline{w} \cdot (r_p^2 - |\underline{b}|^2 - g)^{1/2}$$

$$\underline{p} = \underline{a} + \underline{b} + \underline{c} \qquad (3)$$

Vector $\underline{p}$ describes the position of a point in the geocentric coordinate system. For sea ice drift studies, it is helpful to work in a map projection rather than with 3-dimensional coordinates. In the present paper, we will use an orthogonal projection onto a plane which is tangent at the Earth's surface in the center point of an area of interest.

2.2 Sweep Delay c and Scale Factor f (Eq. 2)

The JPL L-Band radar system images the nadir, thus the area underneath the aircraft, and out to about 55° off-vertical. The image of the nadir can be used for field calibration of the sweep delay c and of the scale factor f of Eq. (2). For this purpose, the range r_n of a nadir point is compared with the radar altimeter reading a_n from the recordings of the aircraft positions. Differentiation of Eq. (2) shows, that difference:

$$\Delta r_n = r_n - a_n = (y'_n + c) \cdot \Delta F + f \cdot \Delta c + f \cdot e'_y - e_a \qquad (4)$$

Equation (4) illustrates that the discrepancy Δr_n can be the result of erroneous constants c or f, and of course of errors e_y and e_a in measuring the altitude a_n and image coordinate y'_n.

If it can be assumed that e_a, e_y are random errors of mean zero, then a least squares adjustment using a number of nadir measurements allows for the computation of Δf and Δc, provided of course that the flight altitude and thus y'_n are varying over a sufficiently wide range to permit separation of Δf and Δc. If the flight altitude is constant, then so is y'_n and Δc, Δf cannot be separated. Instead, Δf has to be assumed to be zero, and only Δc can be computed.

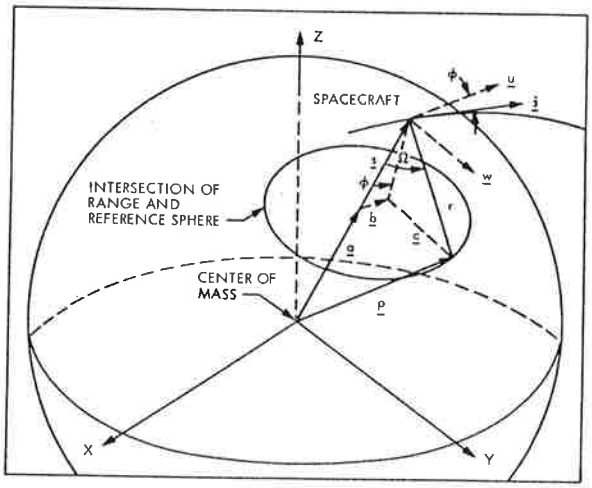

Figure 3:
Definition of the coordinate system and vectors relevant to radargrammetric computations. Vector $\underline{w}$ is normal on $\underline{s}$ and $\dot{\underline{s}}$; vector $\underline{u}$ is normal on $\underline{s}$ and $\underline{w}$; vector $\underline{b}$ is parallel to $\underline{m}$; and vector $\underline{c}$ is parallel to $\underline{w}$.

In the present configuration of the L-band radar, the range reference line is only very weakly defined in the image (see fig. 2) and the scale factor f has as yet not been calibrated in the laboratory. A field calibration of the constants c and f was therefore required for the present analysis. In the case, however, where both constants c and f are known with a high accuracy and where a well defined range reference line is available, the nadir returns should not be used to correct the radargrammetric range measurements, but instead to correct the recordings of the flight altitude.

2.3 Ground Control Points

If points are identifiable in the radar imagery whose ground coordinates are known, then it is possible to compare radargrammetric coordinates with the given ground coordinates. The differences can be used to correct all radargrammetric coordinates (interpolative approach). An alternative is to compare the time of imaging, t_p, and range r_p obtained from the radar image with the values resulting from the ground coordinates, and then applying corrections to t_p and r_p (parametric approach). Both the interpolative and parametric use of known ground control points have been described in a previous radargrammetric study of lunar mapping (Leberl, 1975b). Reference is made to this study for an explanation of the methods of using ground control points.

2.4 Filtering of Measurement Errors of Inertial Navigation

It was pointed out that the position vector $\underline{s}$ and velocity vector $\dot{\underline{s}}$ of the sensor are required as an input to the radar coordinate transformation of Eq. (3). These vectors $\underline{s}$, $\dot{\underline{s}}$ are obtained from recordings of the inertial navigation data. However, original measurements taken from the inertial guidance system can be quite erroneous. To eliminate some of the effects of these errors, it is necessary to filter particularly the high-frequency noise. This can be achieved by smoothing the original measurements (low-pass filter). A weighted moving average algorithm was employed, and its parameters were experimentally optimzed using radar

images taken over land. The best results were obtained by rather drastic smoothing, using a second order moving average and employing data points over a flight period of 3 minutes of time (measurements were recorded every 10 seconds). For best results, no weighting was applied (flat point spread function).

3. EXPERIMENTAL EVALUATION OF DRIFT MEASUREMENTS USING IMAGES OF LAND FEATURES

The accuracy with which sea ice drift can be measured from airborne radar images can be evaluated from images of a non-moving, well-mapped surface. A number of ground control points on a plane and horizontal land surface in the vicinity of Prudhoe Bay, Alaska, are thus used for this purpose. The geographical coordinates for the ground points were scaled off the 1:250,000 scale topographic map of Alaska (accuracy about $\pm$ 2µm). This land based experimental calibration is thus similar to the one applied by Hibler et al., (1975) prior to the use of LANDSAT images for measurements of sea ice drift.

igures 4a and 4b illustrate the distribution of about 20 ground control points imaged during two different flights along the meridian of longitude $\lambda = 149° 15'$. These figures also show the differences between radargrammetric and ground control points. Figure 4c then shows the apparent drift that is obtained from two sequential radar images. The errors in both the radargrammetric coordinates as well as drift measurements are highly systematic and large, since the images were flown on different days, and both about 5 hours after take-off; inertial navigation errors have accumulated. However, in figures 4d, 4e and 4f, only one ground control point is used to eliminate the constant component of the errors. Table 1 describes quantitatively the error reduction when one, two or four ground points are used to correct the mapping result in an interpolative procedure. It can be concluded from fig. 4 and table 1 that the largest component of the mapping error is only slowly varying and almost constant over a distance of 100km, so that a single known point on the ground drastically reduces the error of mapping and drift measurement. Previous radar mapping studies (V. Roessel et al., 1974; Leberl, 1975a) identified the inertial navigation as the dominant source of radar mapping errors, with sinusoidal error periods of about 1.5 hours ("Schuler period") and an amplitude that can increase with about 0.5 to 1 km per hour of flight. At an aircraft speed of 600 km/hour, this produces sinusoidal navigation errors with a period of 900 km.

It was pointed out in section 2.4, that the high frequency noise of the flight data (inertial navigation recordings) has to be filtered prior to the radargrammetric coordinate transformation. Table 2 presents the apparent relative "drift" of land features when no filtering and two low-pass filters are applied. The filters employ a moving average with, in one case, no weighting of the data points, and in the other case eighting of the data points inversely proportional to the 3rd power of he distance from the estimation point. Table 2 indicates that the best result is obtained when no weighting is applied to the data points.

In conclusion, one can thus assume that sea ice drift can be measured from JPL L-band radar images and the inertial navigation of the NASA CV-990 aircraft with an absolute accuracy depending on the accuracy of the inertial navigation. This amounts in the present example (5 hours after take-off) to about $\pm$ 3 km per image pair. The relative accuracy of drift measurements is much higher, namely about 0.1 to 0.2 km per image pair. If strain, strain rates and vorticity are to be computed, it is this relative accuracy which is significant.

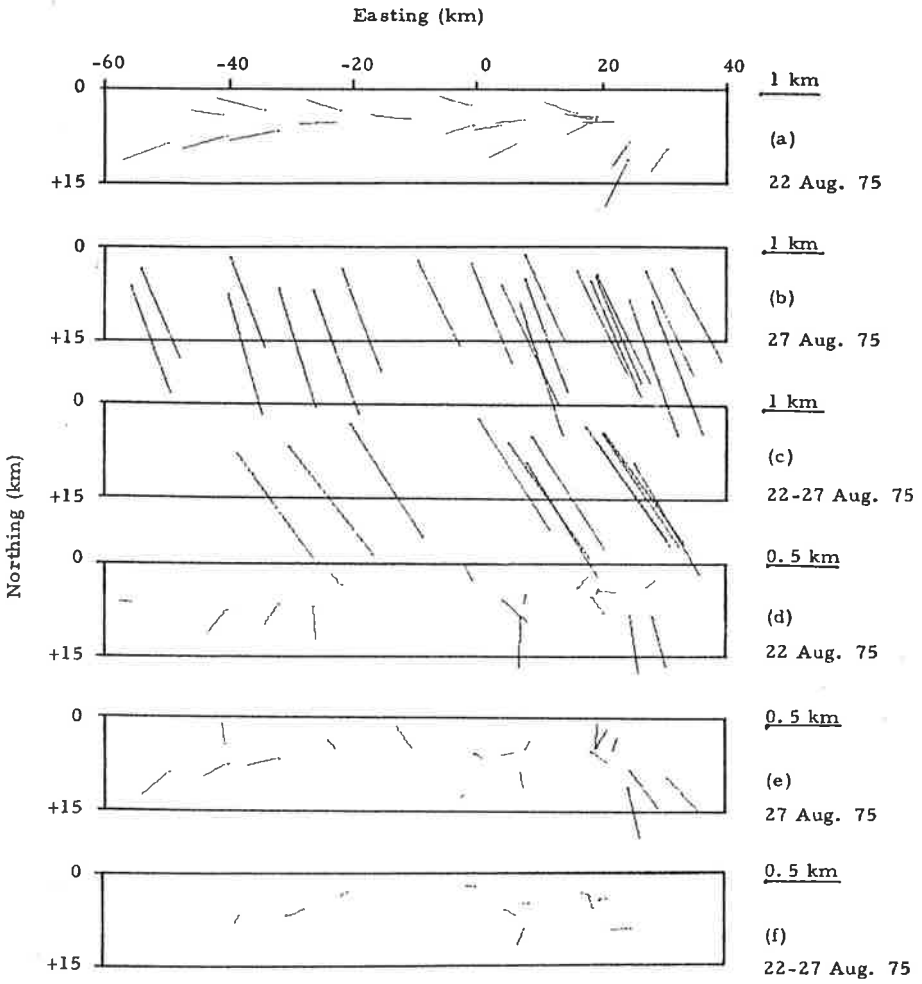

Figure 4:

Distribution of ground control points imaged during two separate flights over Prudhoe Bay, Alaska, with (a) and (b) difference vectors between radargrammetric and map coordinates; (c) apparent "drift" of ground control points; (d), (e) and (f) as (a), (b) and (c) but without the systematic effect of the inertial navigation error.

R. M. S. DIFFERENCES (KM)						
	GROUND - RADAR 22 August		GROUND - RADAR 27 August		APP. DRIFT 22 - 27 August	
	North	East	North	East	North	East
No Filter	0.51	0.12	0.37	0.12	0.52	0.15
Filter, Weighting	0.34	0.10	0.23	0.12	0.34	0.13
Filter, No Weighting	0.18	0.14	0.13	0.11	0.16	0.11

Table 1: Effect of using raw and filtered flight data on(relative)accuracy of radar mapping, as obtained after least squares linear, conformal fit.

R. M. S. DIFFERENCES (KM)				
No. of Ground Control Points	GROUND - 22 August		GROUND - 27 August	
	North	East	North	East
0	1.07	0.48	1.45	3.50
1	0.27	0.32	0.19	0.29
2	0.19	0.20	0.15	0.23
4	0.18	0.14	0.14	0.09

Table 2: Radar mapping errors when using a different number of ground points to correct the radargrammetric coordinates.

4. AN EXAMPLE OF ARCTIC SEA ICE DRIFT MEASUREMENT FAR FROM LAND

Figures 5a, b and c show a triplet of synthetic aperture L-Band radar images of summer ice taken on 18AUG75, 22AUG75 and 27AUG75 respectively. It is apparent from these three images that there has been drifting of ice floes relative to one another. For example the small lead between the two large multiyear floes (A and B) has closed slightly between the 18th and the 22nd, even though the polynya (C) has retained essentially the same shape.

It is quite evident from this image, also, that the ice has not been subjected to a great deal of pressure (i.e. there are no ridges forming nor has there been any rafting of one floe onto another). Also, the ice movements have been primarily those of drifting (note small floes at point D) primarily within the polynya. In such cases, the shapes of the floes have remained essentially intact, although some minor amount of breaking and smoothing along the sharper edges is evident on the small floes at D. This type of qualitative information, obtained from a visual inspection of the data are helpful in identifying movement on a very local and restricted scale. They are not especially germane however, to the larger question of absolute drift.

Figure 6 illustrates the result of the drift measurements obtained from a pair of radar images (Fig. 5b and 5c). This result leads to the conclusion that the westward drift of the ice was 6.5 km/day, and the northward drift about 2.9 km/day.

The images of the ice floes were taken about 1.5 to 2 hours after take-off of the aircraft from the airport in Fairbanks, Alaska. The inertial guidance errors can thus be expected to be smaller than the errors found in the coastal images of the previous section. The absolute errors of the drift measurements can thus be estimated to amount to about 200 m/day or about 5%.

However, the error due to the inertial navigation is constant in the area of interest. The differential (relative) drift can thus be indicated with a much higher accuracy than the absolute drift. In order to demonstrate this, one ice distribution map is shifted and rotated with respect to the other to minimize residual drift values (a least squares linear orthogonal transformation is applied) and thus to eliminate the overall drift and drift measurement errors. Only then are values computed for the displacement and rotation of the individual floes. Figure 7 illustrates the result. It can be noted, that during the 5 days between taking the two radar images, there was a tendency for the individual ice floes to swing around individual vertical axes of rotation. Horizontal differential displacements are apparent, but do not show a distinct trend.

The above approach was based on the use of a comparator for measuring homologuous ice features on sequential radar images, and ice drift values for the few selected measurements were then derived numerically. Instead of this approach, one could also aim at first producing differentially rectified radar images using a digitized version of the images in a digital image processing system, and then obtain drift values graphically from superposed rectified radar images. Figure 8 shows the digitally rectified images produced from the originals that were presented in figure 5 with slant ranges. The rectified radar images do not reveal additional information on sea ice distribution that could not also be extracted directly from the original unrectified images. Certain ice features in the near range area close to the nadir become somewhat easier to recognize. But this advantage is not striking.

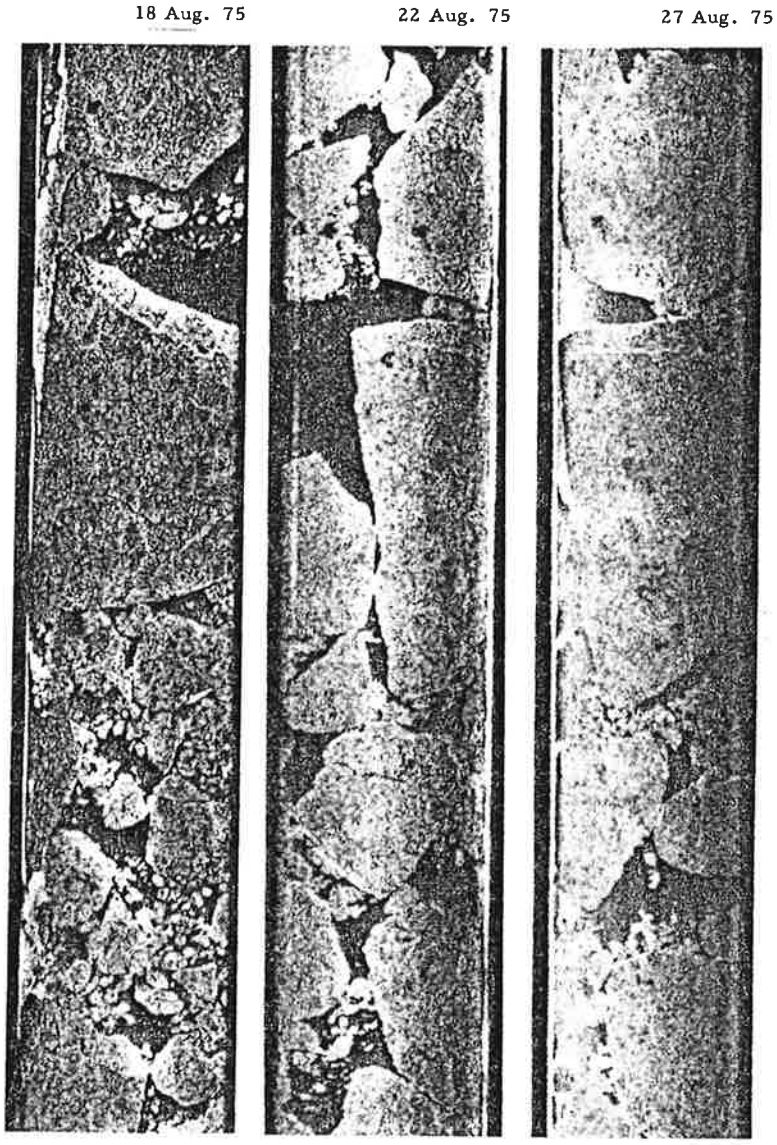

Figure 5: Triplet of sequential radar images of arctic sea ice.

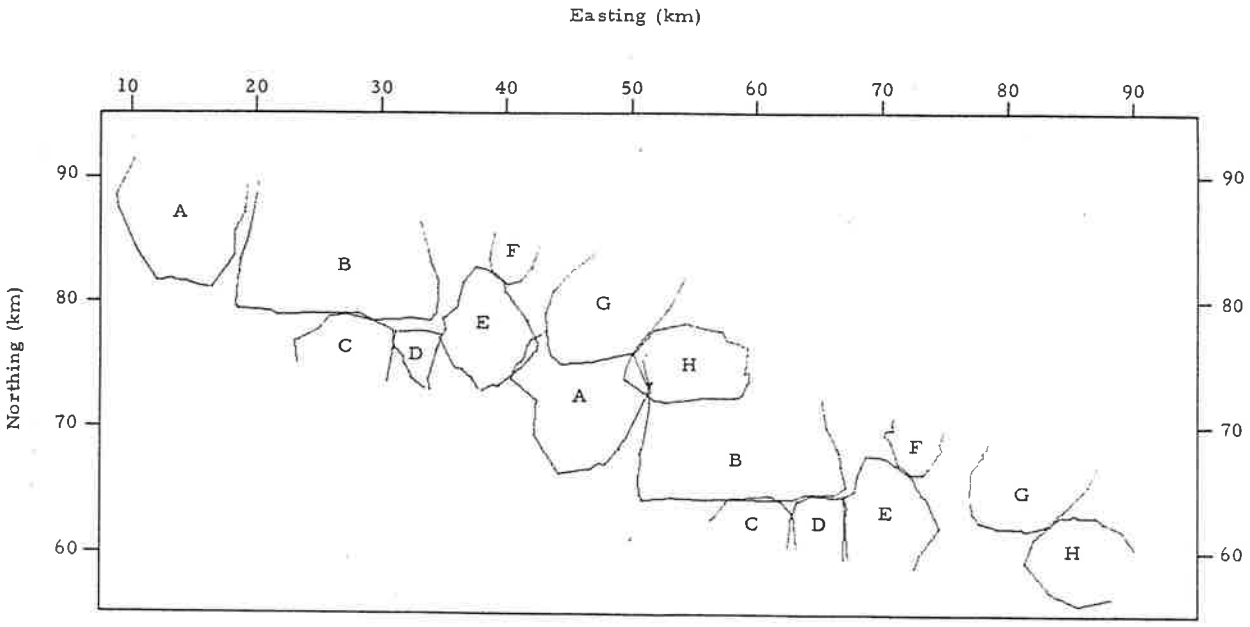

Figure 6: Map showing the distribution of selected ice floes on both the 22nd and 27th of August 1975.

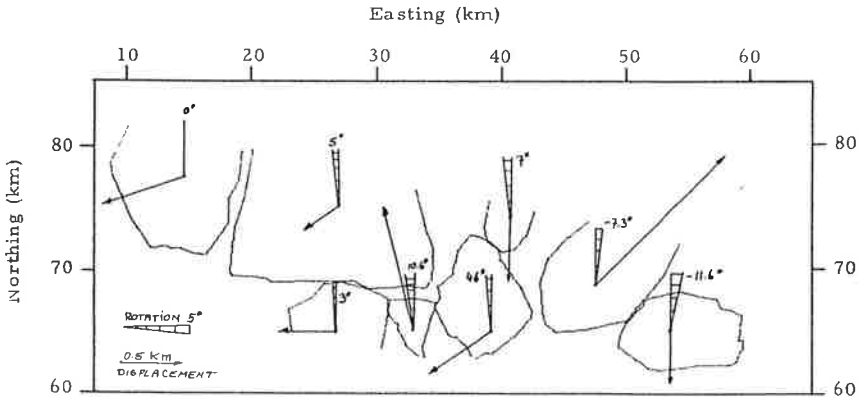

Figure 7:
Differential ice drift derived after linear orthogonal least squares transformation of the later ice map (27th of August) into the early map (22nd of August).

For the purpose of drift measurements, the numerical approach based on comparator measurements is therefore superior: The measurements of ice features can be input to the direct computation of drift, strain rate and vorticity, and can be subject to flexible numerical treatment of measurement errors. The approach of differentially rectifying the radar images is only justified, if the ultimate aim of the effort is the production of an image mosaic in addition to the drift analysis.

A radar image mosaic might be very useful in addressing oneself to the larger problem of the amount and distribution of open water within the Arctic Ocean areas. In this case the use of the 'stretched' imagery (i.e. that which is geometrically corrected) greatly reduces the problems of making area measurements. Area measurements are of major importance from the point of view of heat exchange between the ocean surface and the atmosphere because, as pointed out by Badgley (1966), the heat loss from even small areas of open water is at least two orders of magnitude greater than that from old ice. An accurate determination of the distribution of the open water, thin ice and older (multiyear) ice in the arctic ocean, may be easily obtained by using such radar imagery as discussed in this paper. This would prove to be a valuable input to mathematical modeling and quantitative understanding of the dynamics of the Arctic Ocean ice, the effect of the heat exchange between the ocean the atmosphere and the reflection of solar radiation to the atmosphere from the ice and water surface. The effects of these exchanges have obvious implications on the global circulation of both the atmosphere and the oceans.

The sensitivity of radar mapping to the filtering of errors of the inertial flight data is illustrated in figure 9. The ice floe maps from the 22nd of August 1975 are superimposed in this figure. One map was prepared using flight data that were filtered without weighting of data points; the other map was prepared with weighting inversely proportional to the 3rd power of the distance from the estimation point. Figure 9 shows that the shape of floes is presented differently, with difference amounting to a r.m.s value of $\pm$ 0.1 km.

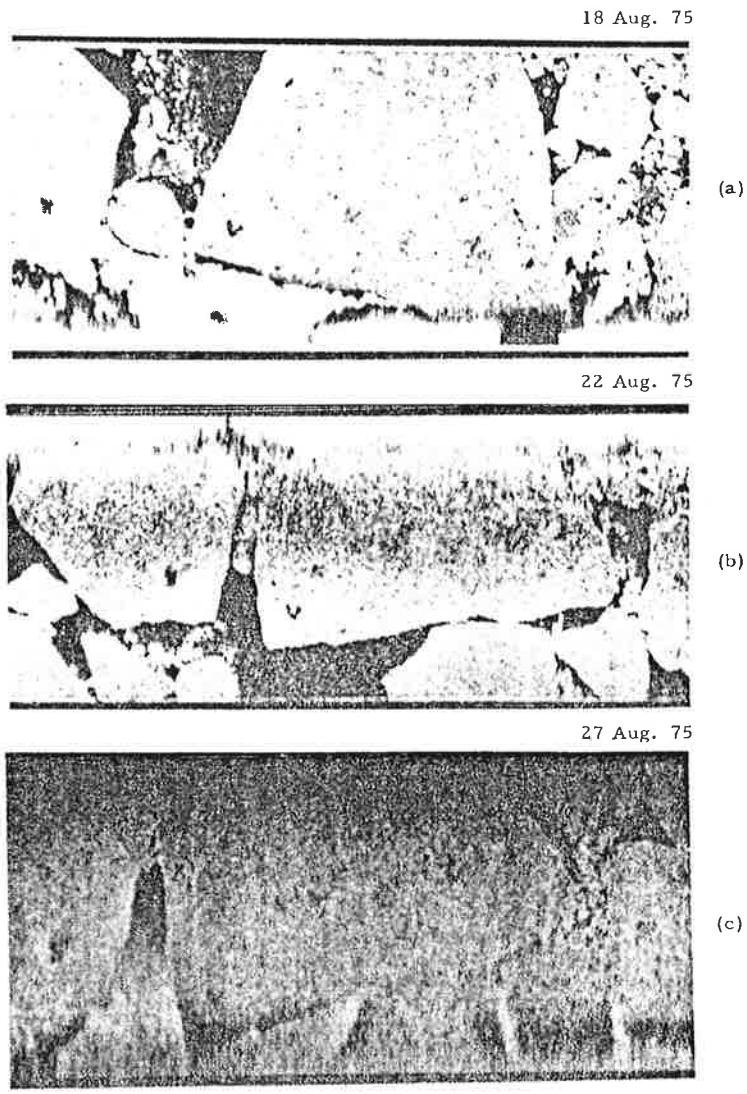

Figure 8:

Digitally rectified radar images. Originals are shown in Figure 5.

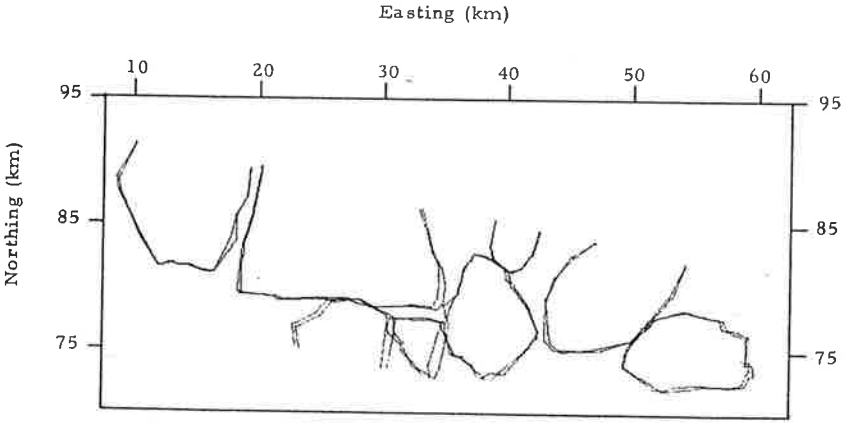

Figure 9:

Superimposed map of ice floes prepared from radar image of 27th of August 1975, but using two different filters for elimination of high frequency noise in the inertial flight data.

5. CONCLUSIONS

We have analyzed in this paper a method of quantitativley mapping sea ice drift at locations far from land using airborne synthetic radar imagery. The accuracy of determining absolute drift and relative motion of ice floes was estimated using radar images of land features. The errors of the absolute drift are dominated by the errors of the inertial navigation with about 0.5 to 1 km per hour of flight.

The error of mapping the relative motion of ice floes is dominated by the inaccuracy of identifying homologuous ice features on images taken at different times, and by the limited geometric regidity of radar image acquisition. An example is presented employing the L-band synthetic radar images produced by the system of the Jet Propulsion Laboratory (JPL). The relative accuracy obtained with this imagery is about 0.1 to 0.2 km. We expect, however, that ths relative accuracy can be further improved by establishing a firm geometric reference in the images (range reference line, range scale factor). Thus far, we have studied ice only from individual radar images and concentrated thus on drift of individual floes. The next step will be the use of an entire block of overlapping radar images. This will require radargrammetric mosaicing of the images and will permit us to expand our study onto mesoscale sea ice drift and deformation over a much larger area.

ACKNOWLEDGEMENT

We gratefully acknowledge the support of Teledyne-Geotronics of Long Beach, California, who made a Wild PUG point transfer device and their Mann-Monocomparator available for use in the present study. We are furthermore grateful to Fred Staudhammer for the digital image processing applied to some of the radar images.

REFERENCES

Anderson, V. H. (1966) "High Altitude Side-Looking Radar Images of Sea Ice in the Arctic," Proceedings of the Fourth Symp. on Remote Sensing of Environment, Ann Arbor, Willow Run Laboratories, Inst. of Science and Technology, University of Michigan.

Badglet, F. (1966) "Heat Budget at the Surface of the Arctic Ocean" Proc. Symp. On Arctic Heat Budget and Atmospheric Circulation, (J. Fletcher, ed). RAND CORP. (RM - 5233-NSF).

Campbell, W. T. et al. (1975) "Geophysical Studies of Floating Ice by Remote Sensing," Journal of Glaciology, Vol. 15, No. 73.

Dunbar, M. (1975) "Interpretation of SLAR Imagery of Sea Ice in Nares Strait and the Arctic Ocean," Journal of Glaciology, Vol. 15, No. 73.

Hibler, W. D. III, et al. (1975) "Techniques for Studying Sea Ice Drift and Deformation at Sites far from Land Using LANDSAT Imagery," Proceedings of the Tenth International Symposium on Remote Sensing of Environment, Environmental Research Institute of Michigan, Ann Arbor Michigan.

Leberl, F. (1975a) "Radargrammetric Point Determination PRORADAM," Bildmessung und Luftbildwesen, Vol. 43, No. 1, W. Germany.

Leberl, F. (1975b) "Lunar Radargrammetry with ALSE-VHF Imagery," Proceedings of the American Society of Photogrammetry," Fall Convention, Phoenix, Arizona.

Roessel, J. van, et al. (1974) "SLAR Mosaics for Project RADAM", Photogrammetric Engineering, Vol. 40, No. 1.